Published OnlineFirst September 14, 2010; DOI: 10.1158/0008-5472.CAN-10-1253

Cancer Research

Nongenomic Effects of Cisplatin: Acute Inhibition of Mechanosensitive Transporters and Channels without Actin Remodeling

Nina Milosavljevic[1], Christophe Duranton[1], Nadir Djerbi[1], Pierre Henri Puech[3], Pierre Gounon[2], Dominique Lagadic-Gossmann[4], Marie Thérèse Dimanche-Boitrel[4], Cyril Rauch[5], Michel Tauc[1], Laurent Counillon[1], and Mallorie Poët[1]

Abstract

Cisplatin is an antineoplastic drug, mostly documented to cause cell death through the formation of DNA adducts. In patients, it exhibits a range of short-term side effects that are unlikely to be related to its genomic action. As cisplatin has been shown to modify membrane properties in different cell systems, we investigated its effects on mechanosensitive ion transporters and channels. We show here that cisplatin is a noncompetitive inhibitor of the mechanosensitive Na^+/H^+ exchanger NHE-1, with a half-inhibition concentration of 30 μg/mL associated with a decrease in V_{max} and Hill coefficient. We also showed that it blocks the Cl^- and K^+ mechanosensitive channels VSORC and TREK-1 at similar concentrations. In contrast, the nonmechanosensitive Cl^- and K^+ channels CFTR and TASK-1 and the Na^+-coupled glucose transport, which share functional features with VSORC, TREK-1, and NHE-1, respectively, were insensitive to cisplatin. We next investigated whether cisplatin action was due to a direct effect on membrane or to cortical actin remodeling that would affect mechanosensors. Using scanning electron microscopy, *in vivo* actin labeling, and atomic force microscopy, we did not observe any modification of the Young's modulus and actin cytoskeleton for up to 60 and 120 μg/mL cisplatin, whereas these concentrations modified membrane morphology. Our results reveal a novel mechanism for cisplatin, which affects mechanosensitive channels and transporters involved in cell fate programs and/or expressed in mechanosensitive organs in which cisplatin elicits strong secondary effects, such as the inner ear or the peripheral nervous system. These results might constitute a common denominator to previously unrelated effects of this drug. *Cancer Res; 70(19); 7514–22. ©2010 AACR.*

Introduction

Cisplatin is an antineoplastic drug used in the treatment of ovary, testes, kidney, or head and neck solid tumors (1). Understanding its mechanisms of action is crucial for the design of adjunctive treatments that prevent resistance and help patients to better tolerate chemotherapy. Cisplatin forms DNA purine-purine adducts (2) that trap proteins of the high-mobility group. These complexes block the enzymatic machinery that acts on DNA and activate pathways that signal genome damage, ultimately leading to cell death (see ref. 3 for review). However, this mechanism cannot explain all the actions of this drug. First, in patients, cisplatin elicits a range of short-term secondary effects that include disturbance of the hydroelectrolytic balance, gastrointestinal troubles, hearing alterations, imbalance, and modified perceptions or sensations. Second, in cellular models, cisplatin acts on microtubules (4) and actin polymerization (5) and can modify or interact with phospholipids (6, 7). Other studies including genetic screens for cisplatin resistance have documented that membrane proteins (8), enzymes involved in lipid synthesis and modification (9), or cellular enzymes (10) are affected by this drug. In this context, we previously reported that cisplatin increases membrane fluidity and activates the acid sphingomyelinase (11, 12). This enzyme converts sphingomyelin to ceramide that plays a key role in the response to a wide range of proapoptotic signals. Because modifications of membrane composition and fluidity directly change its mechanical properties, we decided to investigate whether clinical concentrations of cisplatin (13) could affect the function of mechanosensitive transmembrane channels and transporters. In parallel, we also tested transporters and channels bearing common features with the previous ones while being insensitive to membrane tension.

Authors' Affiliations: [1]Université de Nice Sophia Antipolis, Transport ionique: Aspects normaux et Pathologiques, CNRS UMR 6097, Faculté des Sciences; [2]CCMA, Université de Nice-Sophia Antipolis, Faculté des Sciences, Nice, France; [3]INSERM UMR 600/CNRS UMR 6212, Marseille, France; [4]UPRES EA 4427 SeRAIC (IRSET), University of Rennes 1, Faculté de Pharmacie, Rennes, France; and [5]School of Veterinary Medicine and Science, University of Nottingham, Leicestershire, United Kingdom

Note: Supplementary data for this article are available at Cancer Research Online (http://cancerres.aacrjournals.org/).

N. Milosavljevic and C. Duranton contributed equally to this work.

Corresponding Author: Laurent Counillon, TIANP, UMR 6097, Faculté des Sciences Parc Valrose Université de Nice Sophia Antipolis, 06108 Nice Cedex 2, France. Phone: 33-4-92-07-68-53; Fax: 33-4-92-07-68-50; E-mail: Laurent.Counillon@unice.fr.

doi: 10.1158/0008-5472.CAN-10-1253

Published OnlineFirst September 14, 2010; DOI: 10.1158/0008-5472.CAN-10-1253

We show here that the mechanosensitive Na^+/H^+ exchanger NHE-1 (14–16), K^+ channel TREK-1 (17, 18), and outwardly rectifying chloride channel VSORC (19, 20) are all inhibited by cisplatin. In contrast, the nonmechanosensitive glucose transporter, the background K^+ channel TASK-1 (21), and the Cl^- channel CFTR are not inhibited. These results may provide new clues for understanding important secondary effects of cisplatin.

Materials and Methods

Cell cultures

Fibroblasts from the PS120 cell line expressing either wild-type (WT) NHE-1 or the R327E mutant were grown as described (22). COS cells were grown as described (17). DCT kidney cells were cultured on collagen-coated Petri dishes as described (23).

Measurement of initial rates of NHE-1

Cells seeded on 24-well plates were acidified as described (22). Measurements were performed by 1-minute incubation in the uptake medium at room temperature (22) supplemented with 3 mmol/L LiCl instead of $^{22}Na^+$, followed by four rapid rinses in ice-cold PBS. Cells were solubilized in 1 N nitric acid (trace metal grade, Fisher Scientific), and Li^+ was measured using atomic absorption spectrometry (Zeeman furnace system, Solaar 969, Thermo Optek). NHE-1 initial rates were calculated as the cariporide (10 μmol/L)–sensitive Li^+ accumulation per well divided by protein quantities.

Apart from the experiments presented in Fig. 1A, cisplatin was added for 10 minutes before uptake and maintained throughout the measurements.

Data were compiled using Microsoft Excel software and fitted using the SigmaPlot 2001 program (Jandel). Unless otherwise stated, the experimental points correspond to the compilation of at least five independent experiments, with each experimental point determined at least in duplicate. Error bars are SE. Constants obtained from fitting data are provided with the error of the fits and r^2 goodness-of-fit factors.

[^{3}H]DOG transport

Cells plated on six-well plates were depleted in glucose for 30 minutes and incubated for the last 10 minutes in the same medium containing 60 μg/mL cisplatin. Initial rates of deoxyglucose uptake were then measured at room temperature (10 μCi/mmol, 0.1 mmol/L). Uptake was stopped using four rapid rinses in ice-cold PBS. Cells were then solubilized in 0.1 mol/L NaOH, and radioactivity was counted using scintillation.

Electrophysiologic studies

Whole-cell currents recorded at room temperature (24) were sampled at 2.5 kHz and filtered at 1 kHz. For the Cl^- channels (VSOR and CFTR) and for the K^+ channel (TASK-2), the cells were held at −50 mV, and 400-ms pulses varying from −100 to +100 mV were applied in 20-mV increments. For the K^+ channel studies (TREK-1), a single ramp varying from −100 to +100 mV in 400 ms was imposed to the clamped cells according to Maingret and colleagues (25). Cl^- current recordings were performed using a pipette solution containing 145 mmol/L NMDGCl, 10 mmol/L HEPES (pH 7.4), 5 mmol/L MgATP, and 5 mmol/L EGTA (Pos = 290 mOsm/kg H_2O). The hypertonic bath solution contained 140 mmol/L NMDGCl, 10 mmol/L HEPES (pH 7.4), 5 mmol/L MgATP, 5 mmol/L EGTA, and

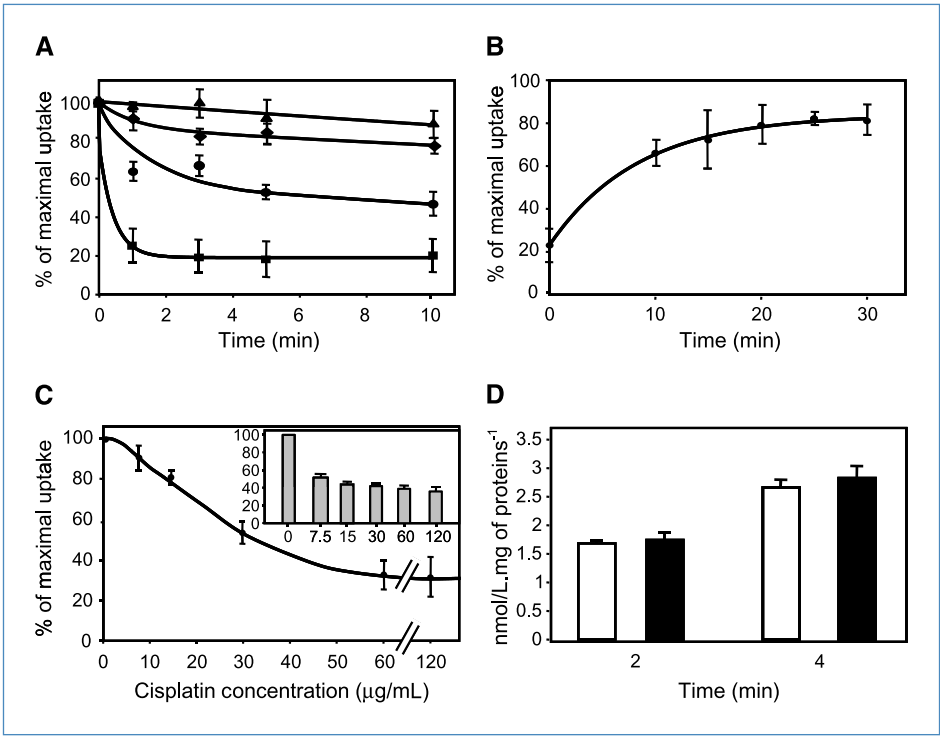

Figure 1. Dose-response and time course of cisplatin inhibition of initial rates of the Na^+/H^+ exchanger NHE-1. Initial rates were measured using fast kinetics of Li^+ uptake, and results are expressed as % of maximal uptake measured in the absence of cisplatin. A, time course of NHE-1 inhibition following incubation with 7.5, 15, 30, and 60 μg/mL of cisplatin. B, recovery of NHE-1 activity after different times of rinse following 10-min incubation with 60 μg/mL cisplatin. C, dose-response curve of NHE-1 inhibition for different concentrations of cisplatin. Inset, dose-response curve for cells exposed to a hypertonic medium (500 mOsm/L). D, effect of 60 μg/mL (dark bars) cisplatin on the initial rates of Na^+-coupled glucose transport.

Published OnlineFirst September 14, 2010; DOI: 10.1158/0008-5472.CAN-10-1253

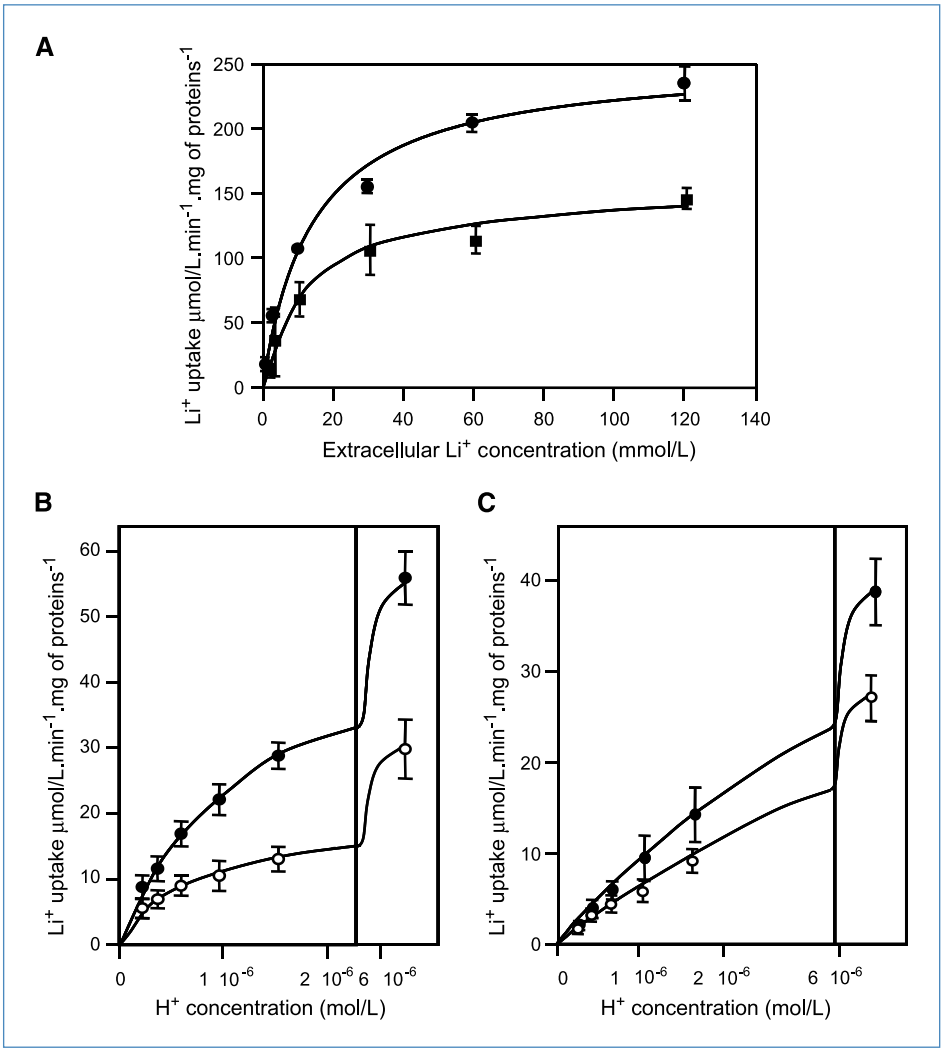

Figure 2. Cisplatin is a noncompetitive inhibitor of NHE-1. A, dose-response curve of initial rates of Li^+ uptake in the presence and absence of 30 µg/mL cisplatin measured as described in Materials and Methods. B, dose-response curve of the WT NHE-1 at different intracellular H^+ concentrations in the absence (●) and presence (○) of 30 µg/mL cisplatin. C, dose-response curve of the Michaelian R327E mutant NHE-1 at different intracellular H^+ concentrations in the absence (●) and presence (○) of 30 µg/mL cisplatin.

50 mmol/L mannitol (Pos = 320 mOsm/kg H_2O). The hypotonic bath solution was obtained by removing mannitol from the previous NMDGCl bath solution.

To study K^+ conductances, pipette and bath compositions were designed to record only K^+ ions movements at positive potentials. The pipette solution contained 140 mmol/L K-gluconate, 10 mmol/L HEPES (pH 7.4), 10 mmol/L EGTA, 1 mmol/L $CaCl_2$ (free calcium concentration of 10 nmol/L), and 1 mmol/L MgATP (Pos = 290 mOsm/kg H_2O). The bath solutions were slightly hyperosmotic and contained 145 mmol/L NaCl or 145 mmol/L K-gluconate, 10 mmol/L HEPES (pH 7.4), 5 mmol/L glucose, 1 mmol/L $CaCl_2$, 1 mmol/L $MgCl_2$, and mannitol (Pos = 320–330 mOsm/kg H_2O).

Electron microscopy

After treatment, cells were fixed *in situ* at room temperature with 1.6% glutaraldehyde in 0.1 mol/L phosphate buffer (pH 7.5). They were then postfixed with 0.5% osmium tetroxide and 0.5% potassium ferricyanide in 0.1 mol/L cacodylate buffer, dehydrated with ethanol, and treated with hexamethyldisilazane before air drying. Samples were coated with 3-nm gold-palladium and observed with a Jeol 6400F scanning electron microscope.

Atomic force microscopy

Micromechanical experiments were conducted with an atomic force microscopy (AFM; Nanowizard I, JPK Instruments) mounted on an inverted fluorescence microscope (Zeiss Axiovert 200; refs. 26–30). Measurements were performed on cells seeded on 24-mm glass coverslips in a heating observation chamber (Biocell, JPK Instruments), which allowed us to carry on the experiment at 25.0 ± 0.1°C. Bright-field contrast imaging was used to select cells, position the cantilever, and monitor cell morphology during measurements. The AFM head was equipped with a 15-µm z-range linearized piezoelectric ceramic scanner used in closed height feedback mode (28) and an IR laser. The sensitivity of the optical lever system and cantilever spring constant was calibrated *in situ*

Published OnlineFirst September 14, 2010; DOI: 10.1158/0008-5472.CAN-10-1253

using built-in routines of the JPK (31). The calibration procedure for each cantilever was repeated up to three times. Spring constants were consistent with the manufacturer's nominal value (10 pN/nm, MSCT/MSNL, Veeco Instruments). The speed for inserting or removing the tip from the cell surface was set to 1 μm/s and the desired contact force to 1 nN. One thousand and twenty-four points per second were used over a travel distance of 4 μm. The contact time was set to 0 to minimize potential dissipation contributions. At least 10 successive force curves were obtained from each cell. Each resulting curve was examined and processed using the JPK-IP batch processing procedures (JPK Instruments): correcting for baseline shift and/or tilt for the pushing part of the force curve, finding the contact point between the tip and the cell, calculating the tip sample separation distance, and fitting the pressing part of the force curve with a Hertz model for a square-based pyramid (31, 32). We then extracted the value of the Young's modulus (E) for each measurement. E values for each cell were pooled to calculate average values that were pooled to gain the distribution of E for each condition. We chose to plot our data as whisker plots because the median is a good estimator of the central tendency of the observed (non-Gaussian) distributions of E modulus. Significance tests were run using nonparametric analysis followed by Dunn tests using Prism (GraphPad Software).

Results

Cisplatin and Na^+-coupled transport

Inhibition of the Na^+/H^+ exchanger NHE-1 is dose dependent and reversible. Figure 1A shows kinetics of inhibition of NHE-1 activity by increasing doses of cisplatin, measured using initial rates of Li^+ uptake (see ref. 22, Materials and Methods, and Supplementary Materials and Methods). Cisplatin inhibition was dose and time dependent, reached its maximal level after 5 minutes (Fig. 1A), and then remained constant. The half-inhibition was estimated as ~30 μg/mL by plotting the dose-dependent inhibition after 10-minute treatment (Fig. 1A and B). Higher doses of cisplatin did not significantly further decrease NHE-1 activity (Fig. 1B). In hypertonic conditions (500 mOsm/L), the half-maximal inhibition was shifted to lower doses of cisplatin (Fig. 1B, inset).

Because cisplatin can form stable molecular complexes, we next investigated the reversibility of this inhibition. Fibroblasts were preincubated for 10 minutes with 60 μg/mL cisplatin and then changed to cisplatin-free medium for various durations before measurements. As shown in Fig. 1C, the effect is reversible over a few minutes, consistent with the observation that inhibition stops to increase shortly after cisplatin addition (Fig. 1A). The curve fitted with a triple exponential, suggesting complex on and off mechanisms.

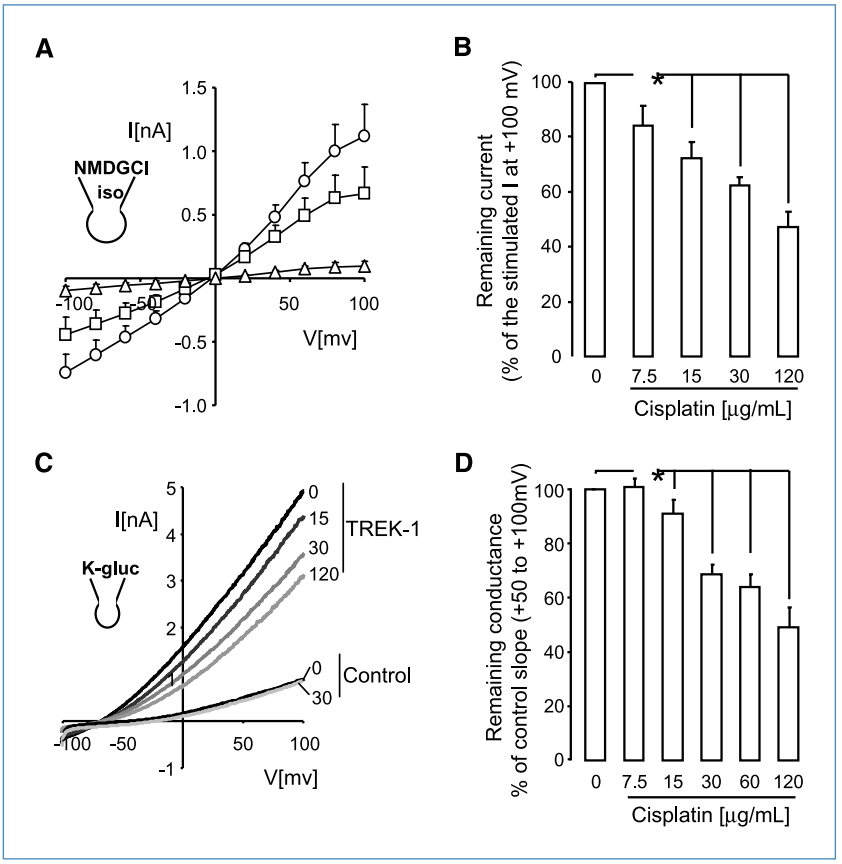

Figure 3. Effect of cisplatin on the VSORC (A and B) and the TREK-1 (C and D) whole-cell currents. A, mean I/V relations between −100 and +100 mV (±SE, n = 9) of whole-cell current recorded in control condition (Δ) 10 min after perfusion of a hypotonic solution alone (○) or with 30 μg/mL cisplatin (□). Current values were analyzed between 350 and 375 ms of each square pulse. B, dose response of cisplatin on the VSORC Cl^- current recorded at +100 mV. Values are expressed in % of remaining currents recorded at cisplatin concentrations of 7.5, 15, 30, and 120 μg/mL and compared with the maximal stimulated current recorded in the absence of cisplatin. Columns, mean of four to nine measurements; bars, SE. *, $P < 0.05$, Student's t test. C, I-V curves elicited by voltage ramps with increasing concentrations of cisplatin (0–120 μg/mL) on the native K^+ current of nontransfected cells (WT, bottom traces) and on the TREK-1 current of transfected COS cells (top gray traces). The pipette was filled with K-gluconate solution and the bath contained NaCl salts. D, histogram representing the effects of increasing concentrations of cisplatin on the TREK-1 K^+ current of COS-transfected cells. Values (±SE, n = 4–9) are normalized to the maximal slope conductance recorded between +50 and +100 mV in control condition (absence of cisplatin) and after addition of cisplatin. *, $P < 0.05$, Student's t test.

Published OnlineFirst September 14, 2010; DOI: 10.1158/0008-5472.CAN-10-1253

To verify that this inhibition was not due to a nonspecific effect that would have affected Na^+-coupled transporters at large, we next tested the effect of 60 μg/mL cisplatin on glucose transport in the same fibroblasts. Initial rates of [^{3}H] DOG (10 μCi/mmol, 0.1 mmol/L) were compared in the presence or absence of 60 μg/mL cisplatin. Figure 1D shows that initial rates of DOG transport measured at 2 and 4 minutes are not affected by 60 μg/mL cisplatin.

Inhibition of NHE-1 is noncompetitive with extracellular cations. We next tested the effect of cisplatin on NHE-1 interaction with its extracellular coupling cations. We measured initial rates of exchange at different extracellular Li^+ concentrations (see Materials and Methods) on the WT NHE-1 with or without 30 μg/mL cisplatin (Fig. 2A). The dose-response curves fitted with Michaelis-Menten kinetics. Cisplatin did not yield significant changes in the K_m values for extracellular Li^+ (12.2 ± 0.2 and 12.5 ± 0.5 mmol/L Li^+ for 0 and 30 μg/mL cisplatin, respectively) but triggered a significant decrease in V_{max} values (270 ± 7 to 142 ± 15 nmol/L.min^{-1}.mg of proteins^{-1}) for Li^+. This shows that cisplatin works as a noncompetitive inhibitor with respect to extracellular cations.

Cisplatin and cooperative regulation of NHE-1 by intracellular pH. Figure 2B shows the effect of 30 μg/mL cisplatin on the dose-response curves of NHE-1 for various clamped intracellular H^+ values, as described by Lacroix and colleagues (22). Because H^+ interacts cooperatively with NHE-1, we fitted these curves with equations corresponding to different possible types of inhibition for a cooperative mechanism: (*a*) a decrease in the V_{max} of the exchanger with no change in cooperativity, (*b*) a decrease in Hill coefficient with a similar V_{max}, and (*c*) a change in the microscopic affinities for protons. All yielded equally good fits (Rsq > 0.9). To discriminate between these mechanisms, we measured cisplatin inhibition on the Michaelian R327E mutant (22) based on the rationale that any mechanism affecting only cooperativity would not affect this mutant, whereas any mechanism affecting either V_{max} or proton binding would also inhibit this mutant. As shown in Fig. 2C, cisplatin decreases its V_{max} measured at 3 mmol/L extracellular Li^+ (59 ± 4 to 37 ± 4 nmol/L.min^{-1}.mg of proteins^{-1}) but does not modify its K_m for intracellular protons (K_m = 8 × 10^{-6} ± 0.5 × 10^{-6} mol/L to 7 × 10^{-6} ± 0.8 × 10^{-6} mol/L; Rsq > 0.97).

Based on these results, we fitted our data for WT NHE-1 with a decreased V_{max}. Interestingly, this fit also yielded a slight decrease in cooperativity, with the following constants: V_{max} = 55 ± 9 nmol/L.min^{-1}.mg of proteins^{-1} and nH = 1.3 ± 0.4 (Rsq = 0.96) in the absence of cisplatin and V_{max} = 29 ± 5 nmol/L.min^{-1}.mg of proteins^{-1} and nH = 1.1 ± 0.4 (Rsq = 0.92) in the presence of 30 μg/mL cisplatin.

Cisplatin and ion channels

Effect of cisplatin on the mechanosensitive VSORC Cl^- conductance and TREK-1 K^+ channel. The effect of cisplatin was tested on the swelling-activated Cl^- conductance VSORC measured as described in Materials and Methods. In control conditions, the voltage step protocol elicited low whole-cell currents with a cord conductance (between +60 and +100 mV)

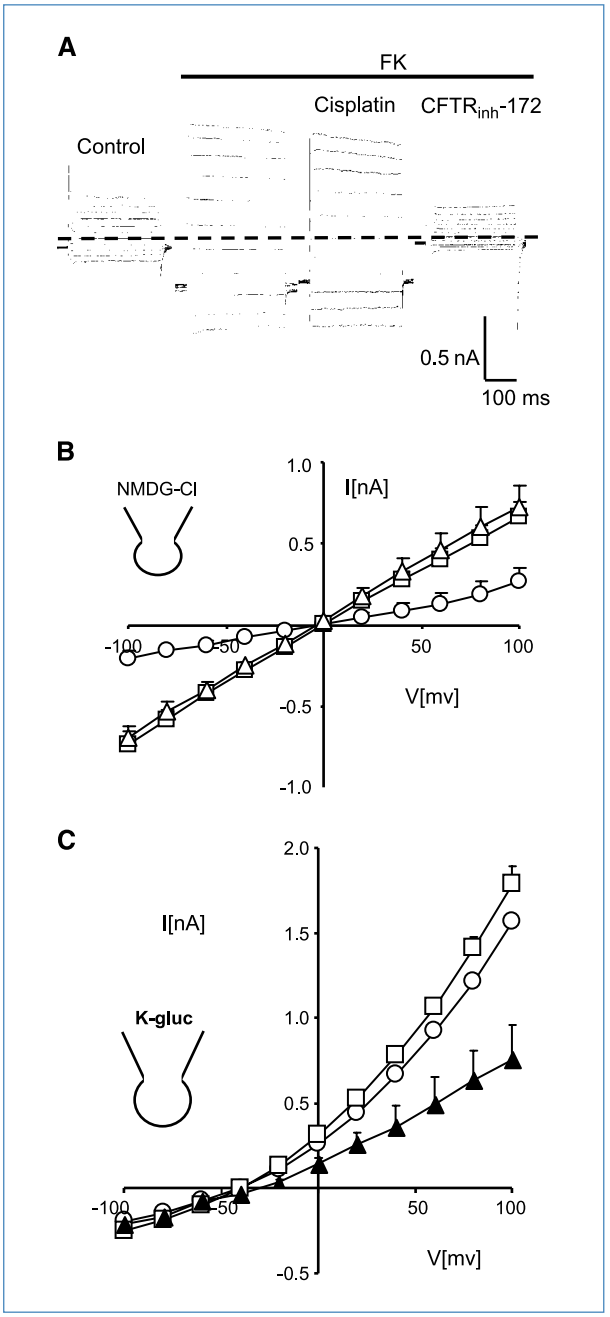

Figure 4. Effect of cisplatin on CFTR (A and B) and TASK-1 (C) whole-cell currents. A, whole-cell current traces recorded in control conditions and 10 min after forskolin exposure (10 μmol/L) in the presence or absence of cisplatin (60 μg/mL). The specific inhibitor $CFTR_{inh}$-172 (5 μmol/L) was applied to confirm that the forskolin-induced current is supported by CFTR activation. B, mean I/V relations (±SE, *n* = 4) recorded as in C, in control condition (○), after 10 min of forskolin exposure (10 μmol/L, △), and finally in the presence of cisplatin (60 μg/mL, □). C, mean I/V relations (±SE, *n* = 4) of whole-cell current recorded in TASK-1–transfected COS cells in control condition (□), in the presence of cisplatin (60 μg/mL, ○), and at pH 6 (▲). The pipette was filled with K-gluconate solution and the bath contained NaCl salts. The currents were elicited by a train of 11-V steps between −100 and +100 mV.

Published OnlineFirst September 14, 2010; DOI: 10.1158/0008-5472.CAN-10-1253

of 0.6 ± 0.3 nS. Exposure to a hypotonic bath solution (260 mOsm/L) induced a Cl^- current that exhibited kinetic and biophysical profiles of VSORC (24). Cisplatin was then perfused and current amplitudes were recorded after 2 minutes. Figure 3A shows the corresponding I/V curves recorded in control condition (triangles) after 10 minutes of hypotonic solution exposure (circles) and after addition of 30 μg/mL cisplatin to the hypotonic solution (squares). The maximal conductance, 8.9 ± 2.7 nS (n = 9), decreased to 4.2 ± 2.3 nS in the presence of 30 μg/mL cisplatin. The dose dependency of inhibition of VSORC was then analyzed in paired experiments (n = 4–9) at +100 mV for 7.5 to 120 μg/mL cisplatin (Fig. 3B). This inhibition was rapidly reversible and was also observed in the NHE-1–deficient PS120 cells, ruling out an indirect effect in which cisplatin inhibition of VSORC would be caused from that of NHE-1 (data not shown).

We next examined the effect of cisplatin on the mechanosensitive 2P domain K^+ channel TREK-1 (18), transiently transfected in COS cells (pIRES CD8 vectors, Fugene HD, Promega). Two days after transfection, cells decorated with anti–CD8-coated beads as described by Poet and colleagues (33) were patched, together with several undecorated cells as control. TREK-1–expressing cells exhibited a dramatic increase of the spontaneous conductance (41 ± 12 nS, n = 8, calculated between +50 and +100 mV) compared with nontransfected cells (8.6 ± 0.6 nS, n = 9) and a shift of the reversal potential to negative value as expected for K^+ ions. Addition of cisplatin to the bath solution induced a dose-dependent inhibition of the TREK-1–mediated K^+ currents (Fig. 3D). Cisplatin (30 μg/mL) remained without effect on the K^+ current recorded in nontransfected cells (Fig. 3C). Here, also, cisplatin inhibition was fully rinsable (data not shown).

Effect of cisplatin on nonmechanosensitive Cl^- and K^+ channels CFTR and TASK-1. The effect of cisplatin was then tested in whole-cell experiments on the CFTR Cl^- conductance expressed in DCT cell line (19). The spontaneous Cl^- conductance, 3.5 ± 0.4 nS, increased to 6.6 ± 0.6 nS after forskolin addition (10 μmol/L, n = 4; Fig. 4A and B). The forskolin-activated I/V relationship exhibited a linear profile typical for CFTR and was completely inhibited by the specific inhibitor $CFTR_{inh}$-172 (5 μmol/L; refs. 34, 35). Addition of cisplatin (60 μg/mL) remained without effect on the forskolin-stimulated current (n = 4; Fig. 4A and B).

Cisplatin was next tested on the background 2P channel TASK-1 transfected in COS cells as above. The CD8-decorated cells exhibited a spontaneous cord conductance of 16 ± 2 nS (calculated between +60 and +100 mV, n = 4) that was inhibited by acidification of the bath solution to pH 6, a hallmark typical for TASK-1. In sharp contrast, TASK-1 currents were not significantly modified by cisplatin (60 μg/mL, conductance of 18 ± 3 nS; Fig. 4C).

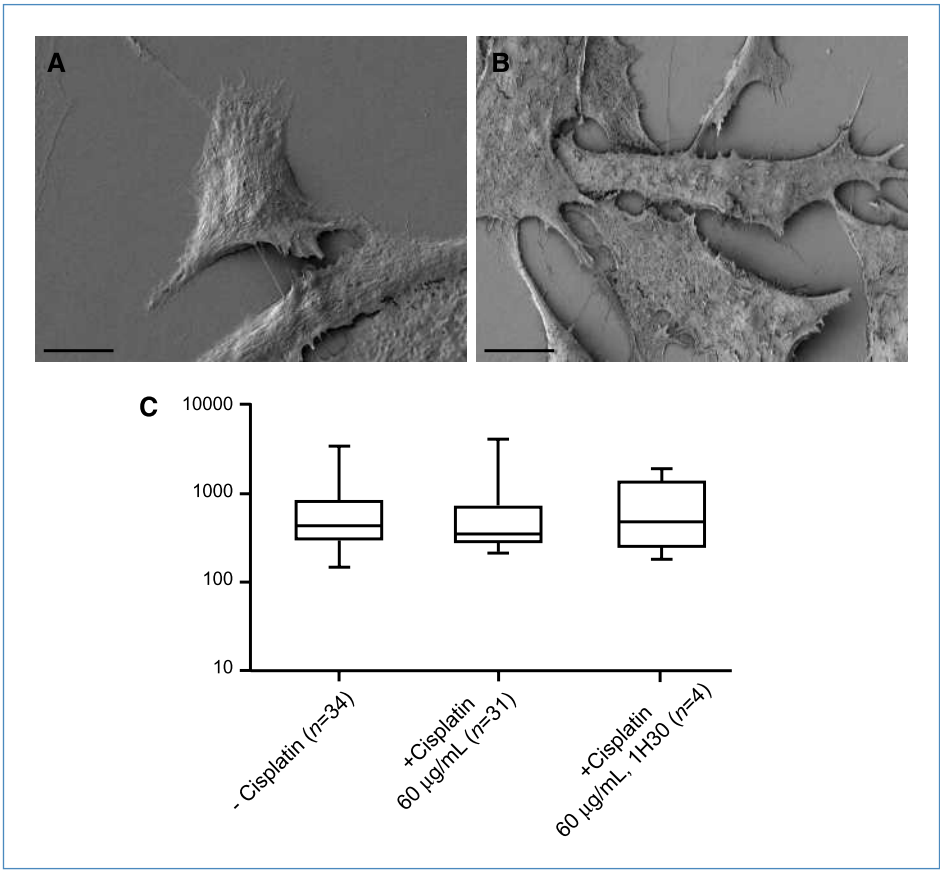

Figure 5. SEM on cisplatin-treated fibroblasts. A, morphologic SEM analysis of fibroblasts in control conditions. B, morphologic SEM analysis of fibroblasts after 10-min incubation in the presence of 60 μg/mL cisplatin. Cells were treated for electron microscopy analysis as described in Materials and Methods. Scale bars, 10 μm. C, AFM micromechanical measurements on adherent cisplatin-treated fibroblasts. Compilation of the Young's modulus values obtained from pressing force curves in the presence or absence of 60 μg/mL cisplatin (see Supplementary Figures for details). Each cell was described by an average Young's modulus value resulting from at least 10 force curves. The whisker plot was obtained by pooling average E moduli from n independent cells for each condition.

Published OnlineFirst September 14, 2010; DOI: 10.1158/0008-5472.CAN-10-1253

Effect of cisplatin on cell shape, actin, and micromechanical properties

Electron microscopy. Figure 5A shows fibroblasts observed in scanning electron microscopy (SEM) in control conditions and following 10 minutes of exposure with 60 cisplatin (Fig. 5B). At 60 μg/mL, cisplatin produced changes in the membrane morphologic features with the appearance of noticeable villosities and long protrusions. These observations, which show a clear modification of membrane shape by cisplatin, were repeated four times with similar results using different batches of cells and cisplatin.

Atomic force microscopy. We next used AFM to measure the Young's modulus of live cells in control conditions and in the presence of 60 μg/mL cisplatin for 10 to 15 minutes. Cells were followed individually, and 10 to 20 pressure curves were recorded before and during the application of cisplatin (see Materials and Methods and Supplementary Materials and Methods). Figure 5C shows that cisplatin application does not significantly change the cell Young's modulus even for long times (Fig. 5C). These results are consistent with an absence of actin remodeling. This is confirmed by *in vivo* actin live imaging (pEGFP-Lifeact plasmid) as shown in Supplementary Fig. S3 (see Supplementary Results).

Discussion

In this study, we show that cisplatin is an inhibitor of the Na^+/H^+ exchanger NHE-1, the K^+ channel TREK-1, and the Cl^- channel VSORC. These three membrane proteins are unrelated in terms of function, structure, ion selectivity, and pharmacologic profiles but share a common feature that is their mechanosensitivity. Despite their biochemical differences, the half-inhibition concentrations of cisplatin were similar for these three channels and transporters, which all exhibited noncanonical dose-response curves. These results point out a common mechanism of inhibition related to membrane tension rather than to protein-ligand interaction. In the same cells and in the same conditions, we could not detect any inhibitory effects of cisplatin on the Na^+-coupled glucose transporter, TASK-1, endogenous K^+ channels, and the CFTR chloride channel that were chosen here because they share biochemical features with those above mentioned, but are not mechanosensitive.

We next decided to investigate in detail the mode of inhibition of one of these targets, the Na^+/H^+ exchanger NHE-1. This transporter constitutes an excellent readout for dissecting complex inhibition mechanisms because a large set of kinetic experiments can be performed on cell populations expressing WT or various mutant exchangers. In contrast with classic NHE-1 inhibitors, cisplatin is not competitive with extracellular cations, does not modify the affinity of the transporter for intracellular protons nor its quantity at the plasma membrane, but decreases its maximal rate and Hill coefficient for intracellular protons. Consistent with the above results, cisplatin inhibition is increased by hypertonic shocks that modify membrane shape and tension.

Cortical actin cystoskeleton is a crucial component of membrane mechanical properties and is connected to mechanosensitive channels and transporters, such as NHE-1 or TREK-1, through their ERM-binding domains (36, 37). In addition, several reports correlated cisplatin effects with actin modifications, but in other cellular systems and for longer treatments than those required for this work (5, 38). Hence, an important question was whether the inhibition of mechanosensitive proteins was caused by a direct effect on membrane or by cortical actin remodeling that would indirectly modify membrane tension or by both. To answer this question, we used a set of different techniques that enabled us to explore possible effects of cisplatin on membrane morphology, cortical actin cytoskeleton, and cell elasticity. Using SEM, we observed that cisplatin provoked the appearance of spikes and villosities, whose number and size increased in a dose-dependent manner. Such structures can be due to direct constraints of the lipid bilayer (see ref. 16 for example) or can also be an early effect of actin depolymerization (39). We next used the Lifeact technique to perform live imaging of actin (40), rather than classic labeling techniques on fixed cell populations, to follow in real time actin evolution on individual cells during cisplatin treatment. For concentrations of 60 and 120 μg/mL of cisplatin, we could not detect any significant change in the actin fibers, or at the edges of the cells, over the time scales used for our measurements (Supplementary Fig. S3). In parallel, we measured cell elasticity using AFM based on the fact that any detectable change in the cell Young's modulus would constitute a direct and quantitative readout of cortical actin modification (39). Here, also, using phase-contrast microscopy, we could follow individual cells before and during cisplatin treatment (Supplementary Fig. S4). Both at 60 and 120 μg/mL, and from 15 to 90 minutes of incubation, we could not detect any significant changes in the cell Young's modulus from pressure curve measurements (Fig. 5C; Supplementary Fig. S4). Taken together, the results obtained by three totally independent and complementary techniques (SEM, actin labeling, and AFM) did not provide any significant evidence that the inhibition of mechanosensitive channels and transporters is due to an effect of cisplatin on cortical actin. Consistently, we could observe with AFM that tube formation on cantilever retraction was occurring more frequently after cisplatin treatment (data not shown), also pointing to a direct effect on the bilayer (26).

As is the case with many efficient drugs, cisplatin exhibits pleiotropic effects that clearly emphasize its action on multiple macromolecular complexes. In this context, our finding that otherwise-unrelated mechanosensitive channels and transporters are affected by this anticancer drug might provide new mechanisms and new targets to explore. First, proteins, such as the Na^+/H^+ exchanger NHE-1, have been shown to be key players in cell life/death decision processes that are crucial in the response to toxic agents and in the efficiency of antineoplastic drugs (see ref. 41 for review). Second, from the results presented here, we can expect that organs that express mechanosensitive proteins to accomplish their functions will be acutely and/or chronically affected by cisplatin. Indeed, there is a large body of examples in which cisplatin elicits rapid effects on its perfusion, which can

Published OnlineFirst September 14, 2010; DOI: 10.1158/0008-5472.CAN-10-1253

eventually be associated with longer-term organ toxicity during treatment. For example, after cisplatin administration, imbalance, tinnitus, and hearing problems associated with longer-term ototoxicity are frequently reported. Obviously, both outer and inner ear rely on mechanosensitive complexes whose components remain to be fully identified. In this context, it is clear that the presence of the cisplatin-inhibited mechanosensitive TREK-1 K^+ channels in the peripheral vestibular system (42) might provide an important clue to these peculiar secondary effects. Indeed, these channels are crucial for the control of endolymph composition and have also been shown to exert neuroprotective effects through their hyperpolarizing action. As well, in patients and in animal models, cisplatin and the related molecules trigger allodynia and cold hypersensitivity (43). This led to the recent study of their transcriptional effects on members of the transient receptor potential (TRP) channels (44) in neurons. Interestingly, Noel and colleagues (45) have recently reported that background mechanosensitive K^+ channels such as TREK-1, which are coexpressed with TRPs, determine the resting potential in sensitive neurons and therefore the threshold for temperature and pain sensation. The inhibition of these K^+ channels by cisplatin might be an area worthy of investigation to understand these side effects, which can be painful enough to interrupt the antineoplastic treatment in patients.

Disclosure of Potential Conflicts of Interest

No potential conflicts of interest were disclosed.

Acknowledgments

We thank Damien Barneaud who participated to this work as a first year Master student; Dr. Edith Garbez (Centre Hospitalier d'Antibes); Nadine Gautier, Chantal Filloux, and Pr. Emmanuel Van Obberghen (U907); Dr. Eric Honoré (IPMC); Pr. Pierre Bongrand (U600/UMR6212); and members of our laboratory Transport Ionique Aspects Normaux et Pathologiques for constant support and fruitful discussions.

Grant Support

Centre National de la Recherche Scientifique and University of Nice-Sophia Antipolis. N. Milosavljevic is funded by the Basileus EMECW project.

The costs of publication of this article were defrayed in part by the payment of page charges. This article must therefore be hereby marked *advertisement* in accordance with 18 U.S.C. Section 1734 solely to indicate this fact.

Received 04/09/2010; revised 06/15/2010; accepted 06/16/2010; published OnlineFirst 09/14/2010.

References

1. Prestayko AW, D'Aoust JC, Issell BF, Crooke ST. Cisplatin (*cis*-diamminedichloroplatinum II). Cancer Treat Rev 1979;6:17–39.
2. Huang H, Zhu L, Reid BR, Drobny GP, Hopkins PB. Solution structure of a cisplatin-induced DNA interstrand cross-link. Science 1995;270:1842–5.
3. Siddik ZH. Cisplatin: mode of cytotoxic action and molecular basis of resistance. Oncogene 2003;22:7265–79.
4. Peyrot V, Briand C, Crevat A, Braguer D, Chauvet-Monges AM, Sari JC. Action of hydrolyzed cisplatin and some analogs on microtubule protein polymerization *in vitro*. Cancer Treat Rep 1983;67:641–6.
5. Kruidering M, van de Water B, Zhan Y, et al. Cisplatin effects on F-actin and matrix proteins precede renal tubular cell detachment and apoptosis *in vitro*. Cell Death Differ 1998;5:601–14.
6. Taylor KD, Goel R, Shirazi FH, et al. Pressure tuning infrared spectroscopic study of cisplatin-induced structural changes in a phosphatidylserine model membrane. Br J Cancer 1995;72:1400–5.
7. Speelmans G, Staffhorst RW, Versluis K, Reedijk J, de Kruijff B. Cisplatin complexes with phosphatidylserine in membranes. Biochemistry 1997;36:10545–50.
8. Grunicke H, Hofmann J. Cytotoxic and cytostatic effects of antitumor agents induced at the plasma membrane level. Pharmacol Ther 1992;55:1–30.
9. Li G, Alexander H, Schneider N, Alexander S. Molecular basis for resistance to the anticancer drug cisplatin in Dictyostelium. Microbiology 2000;146:2219–27.
10. Aggarwal SK, Niroomand-Rad I. Effect of cisplatin on the plasma membrane phosphatase activities in ascites sarcoma-180 cells: a cytochemical study. J Histochem Cytochem 1983;31:307–17.
11. Lacour S, Hammann A, Grazide S, et al. Cisplatin-induced CD95 redistribution into membrane lipid rafts of HT29 human colon cancer cells. Cancer Res 2004;64:3593–8.
12. Rebillard A, Tekpli X, Meurette O, et al. Cisplatin-induced apoptosis involves membrane fluidification via inhibition of NHE1 in human colon cancer cells. Cancer Res 2007;67:7865–74.
13. Laurell G, Andersson A, Engstrom B, Ehrsson H. Distribution of cisplatin in perilymph and cerebrospinal fluid after intravenous administration in the guinea pig. Cancer Chemother Pharmacol 1995;36:83–6.
14. Fuster D, Moe OW, Hilgemann DW. Lipid- and mechanosensitivities of sodium/hydrogen exchangers analyzed by electrical methods. Proc Natl Acad Sci U S A 2004;101:10482–7.
15. Tekpli X, Huc L, Lacroix J, et al. Regulation of Na^+/H^+ exchanger 1 allosteric balance by its localization in cholesterol- and caveolin-rich membrane microdomains. J Cell Physiol 2008;216:207–20.
16. Lacroix J, Poet M, Huc L, et al. Kinetic analysis of the regulation of the Na^+/H^+ exchanger NHE-1 by osmotic shocks. Biochemistry 2008;47:13674–85.
17. Fink M, Duprat F, Lesage F, et al. Cloning, functional expression and brain localization of a novel unconventional outward rectifier K^+ channel. EMBO J 1996;15:6854–62.
18. Maingret F, Patel AJ, Lesage F, Lazdunski M, Honore E. Mechano- or acid stimulation, two interactive modes of activation of the TREK-1 potassium channel. J Biol Chem 1999;274:26691–6.
19. Barriere H, Belfodil R, Rubera I, et al. CFTR null mutation altered cAMP-sensitive and swelling-activated Cl– currents in primary cultures of mouse nephron. Am J Physiol Renal Physiol 2003;284:F796–811.
20. Okada Y. Volume expansion-sensing outward-rectifier Cl– channel: fresh start to the molecular identity and volume sensor. Am J Physiol 1997;273:C755–89.
21. L'Hoste S, Poet M, Duranton C, et al. Role of TASK2 in the control of apoptotic volume decrease in proximal kidney cells. J Biol Chem 2007;282:36692–703.
22. Lacroix J, Poet M, Maehrel C, Counillon L. A mechanism for the activation of the Na/H exchanger NHE-1 by cytoplasmic acidification and mitogens. EMBO Rep 2004;5:91–6.
23. Duranton C, Rubera I, L'Hoste S, et al. KCNQ1 K^+ channels are involved in lipopolysaccharide-induced apoptosis of distal kidney cells. Cell Physiol Biochem 2010;25:367–78.
24. l'Hoste S, Chargui A, Belfodil R, et al. CFTR mediates apoptotic volume decrease and cell death by controlling glutathione efflux and ROS production in cultured mice proximal tubules. Am J Physiol Renal Physiol 2009;298:F435–53.
25. Maingret F, Lauritzen I, Patel AJ, et al. TREK-1 is a heat-activated background K(+) channel. EMBO J 2000;19:2483–91.
26. Krieg M, Helenius J, Heisenberg CP, Muller DJ. A bond for a

Published OnlineFirst September 14, 2010; DOI: 10.1158/0008-5472.CAN-10-1253

lifetime: employing membrane nanotubes from living cells to determine receptor-ligand kinetics. Angew Chem Int Ed Engl 2008;47:9775–7.
27. Puech PH, Taubenberger A, Ulrich F, Krieg M, Muller DJ, Heisenberg CP. Measuring cell adhesion forces of primary gastrulating cells from zebrafish using atomic force microscopy. J Cell Sci 2005;118:4199–206.
28. Puech PH, Poole K, Knebel D, Muller DJ. A new technical approach to quantify cell-cell adhesion forces by AFM. Ultramicroscopy 2006;106:637–44.
29. Taubenberger A, Cisneros DA, Friedrichs J, Puech PH, Muller DJ, Franz CM. Revealing early steps of α2β1 integrin-mediated adhesion to collagen type I by using single-cell force spectroscopy. Mol Biol Cell 2007;18:1634–44.
30. Fierro FA, Taubenberger A, Puech PH, et al. BCR/ABL expression of myeloid progenitors increases β1-integrin mediated adhesion to stromal cells. J Mol Biol 2008;377:1082–93.
31. Franz CM, Taubenberger A, Puech PH, Muller DJ. Studying integrin-mediated cell adhesion at the single-molecule level using AFM force spectroscopy. Sci STKE 2007;2007:pl5.
32. Radmacher M. Measuring the elastic properties of living cells by the atomic force microscope. Methods Cell Biol 2002;68:67–90.
33. Poet M, Tauc M, Lingueglia E, et al. Exploration of the pore structure of a peptide-gated Na^+ channel. EMBO J 2001;20:5595–602.
34. Ma T, Thiagarajah JR, Yang H, et al. Thiazolidinone CFTR inhibitor identified by high-throughput screening blocks cholera toxin-induced intestinal fluid secretion. J Clin Invest 2002;110:1651–8.
35. Noel S, Faveau C, Norez C, Rogier C, Mettey Y, Becq F. Discovery of pyrrolo[2,3-*b*]pyrazines derivatives as submicromolar affinity activators of wild type, G551D, F508del cystic fibrosis transmembrane conductance regulator chloride channels. J Pharmacol Exp Ther 2006;319:349–59.
36. Denker SP, Huang DC, Orlowski J, Furthmayr H, Barber DL. Direct binding of the Na-H exchanger NHE1 to ERM proteins regulates the cortical cytoskeleton and cell shape independently of H(+) translocation. Mol Cell 2000;6:1425–36.
37. Chemin J, Patel AJ, Duprat F, Lauritzen I, Lazdunski M, Honore E. A phospholipid sensor controls mechanogating of the K^+ channel TREK-1. EMBO J 2005;24:44–53.
38. Rebillard A, Jouan-Lanhouet S, Jouan E, et al. Cisplatin-induced apoptosis involves a Fas-ROCK-ezrin-dependent actin remodelling in human colon cancer cells. Eur J Cancer 2010;46:1445–55.
39. Rotsch C, Radmacher M. Drug-induced changes of cytoskeletal structure and mechanics in fibroblasts: an atomic force microscopy study. Biophys J 2000;78:520–35.
40. Riedl J, Crevenna AH, Kessenbrock K, et al. Lifeact: a versatile marker to visualize F-actin. Nat Methods 2008;5:605–7.
41. Lagadic-Gossmann D, Huc L, Lecureur V. Alterations of intracellular pH homeostasis in apoptosis: origins and roles. Cell Death Differ 2004;11:953–61.
42. Nicolas MT, Lesage F, Reyes R, Barhanin J, Dememes D. Localization of TREK-1, a two-pore-domain K^+ channel in the peripheral vestibular system of mouse and rat. Brain Res 2004;1017:46–52.
43. Ta LE, Low PA, Windebank AJ. Mice with cisplatin and oxaliplatin-induced painful neuropathy develop distinct early responses to thermal stimuli. Mol Pain 2009;5:9.
44. Ta LE, Bieber AJ, Carlton SM, Loprinzi CL, Low PA, Windebank AJ. Transient receptor potential vanilloid 1 is essential for cisplatin-induced heat hyperalgesia in mice. Mol Pain 2009;6:15.
45. Noel J, Zimmermann K, Busserolles J, et al. The mechano-activated K^+ channels TRAAK and TREK-1 control both warm and cold perception. EMBO J 2009;28:1308–18.

Published OnlineFirst September 14, 2010; DOI: 10.1158/0008-5472.CAN-10-1253

AACR American Association for Cancer Research

Cancer Research

The Journal of Cancer Research (1916–1930) | The American Journal of Cancer (1931–1940)

Nongenomic Effects of Cisplatin: Acute Inhibition of Mechanosensitive Transporters and Channels without Actin Remodeling

Nina Milosavljevic, Christophe Duranton, Nadir Djerbi, et al.

Cancer Res 2010;70:7514-7522. Published OnlineFirst September 14, 2010.